AIAA JOURNAL
Vol. 40, No. 1, January 2002

Numerical Simulation of the Interaction of Microactuators and Boundary Layers

Duncan A. Lockerby* and Peter W. Carpenter†
University of Warwick, Coventry, England CV4 7AL, United Kingdom
and
Christopher Davies‡
Coventry University, Coventry, England CV1 5FB, United Kingdom

A technique is presented for carrying out relatively low-cost numerical simulations of the interaction between three-dimensional microelectromechanical systems (MEMS)- and mesoscale actuators and a laminar boundary layer. The jet-type actuators take the form of a diaphragm located at the bottom of a cavity. When the diaphragm is driven by piezoceramic, for example, it deflects, reduces the cavity volume, and drives air out of an orifice as a jet into the boundary layer. In an attempt to avoid an inflow phase into the cavity, we study the effects of a "puff-like" jet produced when the diaphragm is driven by a short-duration constant force, or the cavity pressure is suddenly increased by providing air from a microvalve. The theoretical model for the actuator is based on classic thin-plate theory for the diaphragm dynamics and modified unsteady pipe-flow theory for the fluid dynamics in the orifice/nozzle leading to the boundary layer. The cavity fluid dynamics is not modeled in detail; the compressible flow in it is neglected, and the instantaneous pressure there is determined via the perfect gas law. A velocity–vorticity method is used to compute the perturbation flowfield created in the boundary layer. This method is capable of full direct numerical simulations, but for the present results the governing equations were linearized. The cavity and boundary-layer flowfields are linked by requiring continuity of velocity and pressure at the orifice exit. The computational methods are used to investigate such questions as the need for fully interactive computations and the differences between meso- and MEMS-scale actuators.

Nomenclature

b = actuator characteristic dimension
d_c = cavity diameter
d_e = orifice diameter
h = cavity depth
ℓ = orifice length
ℓ^+ = ν/V^+
$\boldsymbol{N}$ = $\bar{\boldsymbol{\Omega}} \times \bar{U} + \omega \times \bar{\boldsymbol{U}} + \boldsymbol{N}'$
$\boldsymbol{N}'$ = $\omega \times \boldsymbol{u}$
p = dynamic pressure
R = $U_\infty \delta^*/\nu$
t = time
t^+ = ν/V^{+2}
$\bar{\boldsymbol{U}}$ = undisturbed boundary-layer velocity
U_∞ = freestream speed
$\boldsymbol{u}$ = (u, v, w), nondimensional velocity perturbation
V^+ = $\sqrt{(\tau_w/\rho)}$
$\tilde{w}_{\text{em}}$ = maximum orifice exit velocity
x = streamwise coordinate
y = spanwise coordinate
z = wall-normal coordinate
δ^* = displacement thickness
μ = dynamic viscosity
ν = kinematic viscosity
ρ = density
τ_w = shear stress at wall
$\bar{\boldsymbol{\Omega}}$ = undisturbed nondimensional boundary-layer vorticity
ω = $(\omega_x, \omega_y, \omega_z)$, nondimensional vorticity perturbation

Subscripts

$\tilde{}$ = quantities in exit orifice flow
e = orifice exit conditions

I. Introduction

IT seems plausible that postponement of separation could be achieved by manipulating the near-wall flow structures in the turbulent boundary layer over the fore section of an aircraft wing. In this case one would seek to enhance the generation of turbulence, which presumably implies increasing the frequency and/or intensity of the turbulent bursting process. The question addressed by our current research program is whether or not such manipulation could be achieved by means of a control system based on microelectromechanical systems (MEMS) actuators and sensors. We will not attempt to answer this question in the present paper. However, the question is relevant here for two reasons. First, the length and timescales of the target near-wall structures ultimately determine the dimensions of the proposed MEMS devices. Second, although the present paper investigates the effects of MEMS actuators on laminar boundary layers, the study is, in a sense, preliminary to addressing this main question.

Commonly accepted estimates[1,2] for the average spanwise streak spacing and bursting frequency for a flat-plate turbulent boundary layer are $100\ell^+$ and $0.004/t^+$. (The wall units are given by $\ell^+ = \nu/V^+$, $V^+ = \sqrt{(\tau_w/\rho)}$, and $t^+ = \nu/V^{+2}$.) These estimates translate approximately to spanwise spacing of 150–300μm and frequency of 20–40 kHz for flight-scale boundary layers on large subsonic aircraft.[1,2] (The commonly used estimate for t^+ just given is based on experiments at laboratory conditions and has not been confirmed at the very different flight conditions.) This suggests that the MEMS actuators should have dimensions of the order of 50–100 μm if they are to manipulate the near-wall flow structures. The present study is concerned in part with the possible use of jet-type MEMS actuators of these dimensions. The type of actuator in question is shown schematically in Fig. 1. Essentially it consists of

Presented as Paper 2000-4330 at the AIAA 18th Applied Aerodynamics Conference, Denver, CO, 14–17 August 2000; received 18 August 2000; revision received 21 May 2001; accepted for publication 14 June 2001.

*Research Associate, School of Engineering, Fluid Dynamics Research Center.
†Professor of Mechanical Engineering, Fluid Dynamics Research Center. Senior Member AIAA.
‡Senior Lecturer, School of Mathematical and Information Sciences.

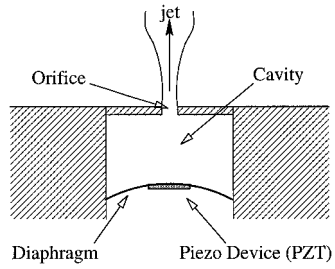

Fig. 1 Schematic sketch of actuator.

a circular diaphragm (made of polymer or silicon) located at the bottom of a plenum chamber that commmunicates with the boundary layer via an orifice or nozzle. The diaphragm would be driven by piezoceramic. This is similar to the type of actuator studied by Rathnasingham and Breuer,[3] Smith and Glezer,[4] Rizzetta et al.,[5] and Crook et al.[6] These investigators have studied relatively small actuators that are, nevertheless, orders of magnitude larger than those needed to control near-wall structures in turbulent boundary layers at flight conditions. Accordingly we have reserved the term MEMS for actuators having dimensions ranging between 1 and 500 μm and used mesoscale for those with dimensions ranging between 0.5 and 50 mm.

One possible mode of operation would be to drive the diaphragm with a periodic voltage so that it oscillates at its resonant frequency. This would produce a so-called synthetic or mass-less jet that, although producing no net mass flow out of the orifice, will nevertheless generate a net jet flow away from the orifice and into the boundary layer by a process akin to acoustic streaming.[4] Mesoscale (as opposed to MEMS-scale) devices of this sort have been shown to be capable of postponing separation by other partners in our research program.[6] (Separation control by means of synthetic jets has also been demonstrated very recently by Amitay et al.[7]) Furthermore, another set of partners has established that oscillatory, as compared with steady, blowing is highly effective for controling boundary-layer separation for a wide range of Reynolds numbers including those typical of flight.[8–10] Another device that produces vortical structures by means of an oscillating slot-jet flow has also been shown to have potential for controlling both laminar-turbulent transition and the near-wall turbulence bursting.[11,12]

Thus there is considerable evidence to suggest that synthetic jets and similar devices can be effective for the sort of flow control in question. There are, however, some practical drawbacks. First, as the size of the MEMS actuators must be very small with diaphragms no more than 100 μm in diameter, their natural frequency will be extremely high, i.e., well in excess of 1 MHz. This can make it difficult to effect control at the much lower turbulent bursting frequency. Against this, there is good evidence that amplitude modulation can be an effective way to overcome this problem.[6,11] Also, this problem could be less serious for the cantilever-type actuators,[11,12] providing they can be made substantially longer than the spanwise streak spacing. Second, synthetic jets require a few oscillations of the diaphragm to beome established; this places a limit on their speed of response for controlling the near-wall streak structures in a turbulent boundary layer. Last, owing to the danger of ingesting dust, aircraft manufacturers are loath to contemplate the use of actuators that have a strong suction phase in their operation cycle. For these reasons, particularly the last, we have mainly investigated an alternative mode of operation whereby the diaphragm is driven with a strong, short-duration, constant force. This results in a sharp rise of pressure in the plenum chamber driving a "puff-like" jet into the boundary layer. We have called this mode of operation *pressure-jump actuation.* Isolated pressure-jump actuation could be used, or a series of such events could be triggered at a given frequency as part of a control process. In fact, pressure-jump actuation could be achieved without the use of a diaphragm at all by supplying air at pressure to the plenum chamber through a MEMS-scale valve system.[1,2] This type of actuation will also be investigated in the present paper.

In the present numerical-simulation study we will investigate the interaction of the jet-type, meso- and MEMS-scale actuators with a laminar boundary layer. We will address a number of issues, which are listed as follows:

How important is it for the simulation to be fully interactive? Previous numerical studies of these and other actuators[13–15] have essentially modeled the actuator as a wall boundary condition that can be fully specified in advance of the calculation. However, the actuator modifies the pressure field in the boundary layer, and this in turn will affect the pressure force opposing the motion generated by the actuator. We will show that when this interaction is fully taken into account the results are significantly different from those obtained with boundary conditions specified in advance.

How should the actuator parameters be chosen to give it the greatest effectiveness with respect to generating perturbations to the boundary layer? We have chosen Tollmien–Schlichting waves as the representative boundary-layer disturbances and will report a parametric study addressing this question with respect to these particular disturbances.

Are there significant differences between meso- and MEMS-scale actuators? The previous studies have been concerned with relatively large devices, the smallest being of the order of millimeters, although much smaller devices are possible using microfabrication.[1,2,4] As just noted, actuators for manipulating the near-wall structures will need to have diaphragms as small as 50 μm in diameter, with orifice diameters of around 5 μm. Such tiny devices can be expected to behave quite differently from the relatively large ones. We will use our simulations based on a laminar boundary layer to investigate this issue.

II. Formulation and Numerical Methods

A. Statement of Problem

Our numerical simulations are based on a novel velocity–vorticity method.[16,17] Lack of space precludes a detailed description. The method was developed to simulate the development of perturbations in two- and three-dimensional boundary layers over rigid and compliant walls. The two-dimensional version of the method is presented in detail in Ref. 16, and full details of the current method are given in Ref. 17. The method has been fully validated against a wide range of established results in flow stability and other topics.

For simplicity we will model the laminar boundary layer as a constant-thickness, incompressible shear flow with an undisturbed, streamwise velocity profile, which corresponds to the Blasius profile. The coordinate system (x,y,z) corresponds respectively to the streamwise, spanwise, and normal directions. The domain is semi-infinite such that $z=0$ defines the lower boundary representing the solid surface plus the jet-type actuator. The actuator is represented by a distribution of unsteady flow velocity over part of the surface $z=0$.

We assume that there is a specified, undisturbed flow, represented by the dimensionless velocity $\bar{\boldsymbol{U}}=(U,0,0)$ and vorticity $\bar{\boldsymbol{\Omega}}=(0,0,\Omega_z)$, where U and Ω_z correspond to the Blasius profile. (The freestream flow speed U_∞ and boundary-layer displacement thickness δ^* are used as reference values for nondimensionalization.) The total dimensionless velocity and vorticity fields are then decomposed into $\boldsymbol{U}=\bar{\boldsymbol{U}}+\boldsymbol{u}$ and $\boldsymbol{\Omega}=\bar{\boldsymbol{\Omega}}+\omega$, where $\boldsymbol{u}=(u,v,w)$ and $\omega=(\omega_x,\omega_y,\omega_x)$ represent perturbations from the prescribed mean flow.

B. Governing Equations

We will consider the governing equations for the perturbation flow variables only. These are divided into two sets. Namely, the primary variables $\{\omega_x,\omega_y,w\}$ and the secondary variables $\{\omega_z,u,v\}$. The secondary variables can be defined explicitly in terms of the former and thus, in principle, eliminated from consideration. It can be shown[17] that the evolution of the three primary variables is governed by the following three equations only:

$$\frac{\partial\omega_x}{\partial t}+\frac{\partial N_z}{\partial y}-\frac{\partial N_y}{\partial z}=\frac{1}{R}\nabla^2\omega_x \tag{1a}$$

$$\frac{\partial\omega_y}{\partial t}+\frac{\partial N_x}{\partial y}-\frac{\partial N_z}{\partial z}=\frac{1}{R}\nabla^2\omega_y \tag{1b}$$

$$\nabla^2 w=\frac{\partial\omega_x}{\partial y}-\frac{\partial\omega_y}{\partial x} \tag{1c}$$

where $\boldsymbol{N}=\bar{\boldsymbol{\Omega}}\times\bar{\boldsymbol{U}}+\omega\times\bar{\boldsymbol{U}}+\boldsymbol{N}'$, $\boldsymbol{N}'=\omega\times\boldsymbol{u}$, and $R=U_\infty\delta^*/\nu$. For the simulations presented in the present paper, the governing

equations are linearized by setting $\boldsymbol{N}' \equiv 0$. Strictly, then, our present approach is only valid provided the perturbations are of small amplitude. Linearized governing equations are only used to make the simulation times manageable. Our method is fully capable of carrying out full direct numerical simulations.

C. Boundary and Integral Conditions

The wall boundary conditions take the form

$$u(x, y, 0, t) = 0 \tag{2a}$$

$$v(x, y, 0, t) = 0 \tag{2b}$$

$$w(x, y, 0, t) = f(x, y, t) \tag{2c}$$

where $f = 0$ except at the actuator exit where it equals the instantaneous jet velocity profile.

The definition of vorticity with use of conditions (2a) and (2b) gives the integral conditions

$$\int_0^\infty \omega_y \, \mathrm{d}z = -\int_0^\infty \frac{\partial w}{\partial x} \, \mathrm{d}z \tag{3a}$$

$$\int_0^\infty \omega_x \, \mathrm{d}z = \int_0^\infty \frac{\partial w}{\partial y} \, \mathrm{d}z \tag{3b}$$

that are fully equivalent to the boundary conditions (2a) and (2b). They can therefore be viewed as constraints on the evolution of the primary variables ω_x and ω_y, respectively.

The inflow boundary conditions take the form of undisturbed flow so that $\omega_x = \omega_y = w = 0$ there. Alternatively a predetermined perturbation form such as a Tollmien–Schlichting wave can be used.[16] The computational domains used in our simulations extended sufficiently far in the streamwise direction that the flow perturbations were negligible at the downstream outflow boundary.

D. Modeling the Actuator Dynamics

Our theoretical model for the dynamics of the jet-type actuator depicted in Fig. 1 has some similarity with those used previously.[3,6] To model the dynamics of the diaphragm, we use classic thin-plate theory implemented via a centered finite difference scheme. In cases where we wish to model the mechanics of a piezoceramic driver, e.g., when making a comparison with the measured characteristics of the actuator,[6] we assume a composite plate.[18] For the present results a homogeneous plate with pointwise forcing has been assumed. When a driving force causes the diaphragm to deflect upward, the volume of the air in the cavity is reduced, and the pressure initially rises and then subsequently drops as the air is forced out through the orifice into the boundary layer. We have ignored the detailed dynamics of the air within the cavity and calculated the pressure there by means of the perfect gas law. Thus the air in the cavity is treated as compressible, but the effects of the compressible flow within the cavity are ignored. This appears to be a reasonable approximation providing that, first, the cross-sectional area of the cavity greatly exceeds that of the exit orifice, thereby ensuring low flow speeds within the cavity; and, second, the air only flows out of the cavity. The first condition is met in all our simulations.

The second condition would not be met for a synthetic jet for which there is periodic inflow into, as well as outflow from, the cavity. The computational simulations of Rizzetta et al.[5] show graphically that during the inflow part of the cycle there is a jet directed into the cavity and accompanying recirculating flow. Evidently, then, neglecting the flow within the cavity could be a poor approximation in this case. Nevertheless our actuator model does predict the optimum actuator parameters reasonably accurately for a synthetic jet[18] when compared with experimental methods.[6] One might expect that only outflow will occur if the diaphragm is driven with a constant force or the pressure in the cavity is suddenly raised. In fact, as will be seen next, it is quite possible for inflow to occur even in these cases. Accordingly, our actuator model will probably not be as accurate as expected in these cases also.

The flow through the exit orifice or nozzle was modeled using unsteady pipe-flow theory. This is tantamount to assuming that the streamlines in the exit orifice are parallel to its axis. Experience suggests that this is an adequate approximation providing the length-to-diameter ratio exceeds unity. Substantial pressure differences (and therefore density differences also) across the orifice need to be taken into account, even though the boundary-layer flow is incompressible. For one-dimensional, compressible, orifice flow the continuity and momentum equations can be written as

$$\frac{\partial \tilde{\rho}}{\partial t} + \frac{\partial \tilde{\rho}\tilde{w}}{\partial \tilde{z}} = 0 \tag{4a}$$

$$\tilde{\rho}\frac{\partial \tilde{w}}{\partial t} + \tilde{\rho}\tilde{w}\frac{\partial \tilde{w}}{\partial \tilde{z}} = -\frac{\mathrm{d}\tilde{p}}{\mathrm{d}\tilde{z}} + \tilde{r}\frac{\partial}{\partial \tilde{r}}\left(\frac{\tilde{\mu}}{\tilde{r}}\frac{\partial \tilde{w}}{\partial \tilde{r}}\right) \tag{4b}$$

where $\tilde{z}$ and $\tilde{r}$ are the axial and radial coordinates, respectively; $\tilde{w}$ and $\tilde{p}$ are the axial velocity and pressure, respectively; and $\tilde{\rho}$ and $\tilde{\mu}$ are the density and dynamic viscosity, respectively. To simplify Eqs. (4a) and (4b), it is assumed that the orifice flow is isothermal and that $\tilde{w}$, $\tilde{\rho}$, and $\tilde{p}$ vary linearly with $\tilde{z}$. Thus Eq. (4b) reduces to the following form at $\tilde{z} = 0$:

$$\rho_c\frac{\partial \tilde{w}_c}{\partial t} + \frac{\rho_c\tilde{w}_c(\tilde{w}_e - \tilde{w}_c)}{\ell} = \frac{p_c - p_e}{\ell} + \tilde{\mu}\tilde{r}\frac{\partial}{\partial \tilde{r}}\left(\frac{1}{\tilde{r}}\frac{\partial \tilde{w}_c}{\partial \tilde{r}}\right) \tag{5}$$

where suffices c and e denote conditions at the orifice entry (from the cavity) and exit (into the boundary layer) respectively. Using the same linear variations with $\tilde{z}$, Eq. (4a) can be integrated with respect to $\tilde{z}$ over the length of the orifice in order to obtain the following relationship between $\tilde{w}_e$ and $\tilde{w}_c$:

$$\tilde{w}_e = \frac{\rho_c\tilde{w}_c}{\rho_e} - \frac{\ell}{2\rho_e}\frac{\mathrm{d}\rho_c}{\mathrm{d}t} \tag{6}$$

Substituting Eq. (6) into Eq. (5) gives the following approximate governing equation for $\tilde{w}_c$:

$$\frac{\partial w_c}{\partial t} + \left(\frac{\rho_c}{\rho_e} - 1\right)\frac{\tilde{w}_c^2}{\ell} - \frac{\tilde{w}_c}{2\rho_e}\frac{\mathrm{d}\rho_c}{\mathrm{d}t} = \frac{p_c - p_e}{\ell\rho_c} + \frac{\tilde{\mu}}{\rho_c}\tilde{r}\frac{\partial}{\partial \tilde{r}}\left(\frac{1}{\tilde{r}}\frac{\partial \tilde{w}_c}{\partial \tilde{r}}\right) \tag{7}$$

The convective term $\tilde{w}\,\partial\tilde{w}/\partial\tilde{z}$ is modeled approximately by the second term on the left-hand side of Eq. (7) in a similar way as in Ref. 3. The inclusion of this term makes the actuator model slightly nonlinear. Equation (7) is solved by means of an implicit, centered, finite difference scheme.

The boundary conditions linking the actuator model to the fluid dynamics require continuity of velocity and pressure between actuator exit and the boundary-layer flow. This is similar to the approach used for compliant walls.[16]

E. Numerical Methods and Their Verification and Validation

Lack of space precludes a detailed description and discussion of the numerical methods. Full details of an earlier two-dimensional version of the velocity–vorticity method are given in Ref. 16, and the three-dimensional version is fully described in Ref. 17. A very brief description of the main aspects of the numerical methods follows. The streamwise variations are discretized using a second-order, centered, finite difference scheme. Spectral Fourier and Chebyshev discretizations are used for the spanwise and wall-normal variations, respectively. For time discretization a fully implict scheme is used for the viscous terms combined with a predictor–corrector scheme for the convective terms.

The velocity–vorticity method has been validated by making extensive comparisons with the results of linear stability theory for the three-dimensional boundary layer over a rotating disk. Some of these comparisons are reported in Ref. 17. Further validation is reported in Ref. 18 where numerical simulations of three-dimensional Tollmien–Schlichting waves and also of the three-dimensional Klebanoff modes, both developing in a flat-plate boundary layer, are compared with the predictions of linear theory. It is also necessary to verify and validate the actuator model. This was done in three main ways in Ref. 18. First, the modeling of the diaphragm dynamics was checked by comparing computed and theoretical natural eigenmodes. A 20-point finite difference scheme was found to be adequate for full resolution of the fourth harmonic. The natural frequency of the diaphragm could also be very accurately predicted.

Second, the numerical modeling of the flow through the exit orifice was verified against classic theoretical results from unsteady pipe-flow theory. Third, as no suitable computational or experimental results appeared to be available for validating the actuator model as a whole, it was used to carry out an extensive design optimization procedure. The aim was to see how well the computed optimal parameters for a synthetic-jet actuator operating in still air agree with those determined empirically by Crook et al.[6] The computed results were in good agreement with those determined empirically. This was rather surprising and suggests that neglecting the flow within the cavity is not such a bad approximation after all.

No previous computer simulations or experiments were available for the validation of the combination of the actuator model and the direct numerical simulation of the boundary-layer disturbances. But extensive tests were undertaken to check that the results were grid and domain independent.[18]

III. Results and Discussion

For all of the results presented here, the undisturbed boundary layer is assumed to have constant thickness, such that $\delta^* = 1$ mm, with a Blasius velocity profile and $U_\infty = 30$ m/s. The Reynolds number is 2×10^3.

It is possible to run the actuator model uncoupled from the boundary layer. The broken line in Fig. 2 plots the variation with time of the resulting centerline jet exit velocity for a particular actuator. This actuator has a diameter $d_c = 250\ \mu$m, depth $h_c = 40\ \mu$m, orifice diameter, $d_e = 24\ \mu$m, and length $\ell = 16\ \mu$m. The force applied to the diaphragm was such that the maximum deflection reached $0.002d_e$, and the time to 95% deflection was 1.44 μs. We also carried out a fully interactive computation for the same actuator whereby the perturbation in the boundary layer and the actuator flow were coupled and computed simultaneously. This is depicted by the solid line in Fig. 2. It is plain that the developing boundary-layer perturbation has a significant effect on the jet velocity. The maximum velocity is about $0.14U_\infty$, which is somewhat high for the use of linearized governing equations. However, despite the slight nonlinearity in the actuator model, the results can be scaled down proportionately if the driving force is reduced. Reservations about the validity of linearization notwithstanding, the simulations suggest that a substantial jet speed can be achieved with very small actuators. Materials like single-crystal silicon can easily withstand very much larger deflections than those assumed here.

The differences between the interactive and noninteractive actuator performances increase as the actuators are made smaller. This is well illustrated in Fig. 3. This shows the results of considering actuator specifications such that $d_c = 50b$, $h_c = 100b$, $\ell = 2.5b$, keeping the initial elevated cavity presure invariant, and optimiszing d_e to produce the largest value of maximum jet exit velocity. For a driven diaphragm the initial pressure rise will stay the same from case to case providing the driving force is scaled so that the diaphragm deflection is proportional to b. In fact, to obtain the results in Fig. 3, we dispensed with the diaphragm and just assumed an instantaneous rise in pressure within the cavity. This is an approximate model for an actuator operated by means of a microvalve. The boundary-layer

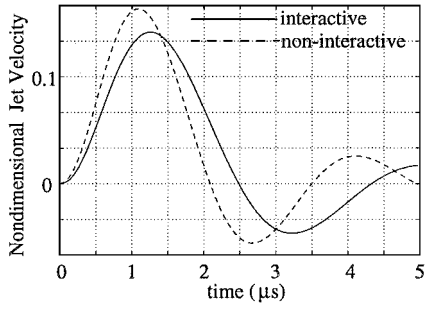

Fig. 2 Variation of nondimensional centerline exit jet velocity with time: ——, actuator alone without interaction with boundary layer; – – –, actuator interacting with boundary layer. Boundary-layer characteristics: $\delta^* = 1$ mm, $U_\infty = 30$ m/s, $R = 2000$. Actuator specifications: $d_c = 250\ \mu$m, $h_c = 40\ \mu$m, $d_e = 24\ \mu$m, and $\ell = 16\ \mu$m.

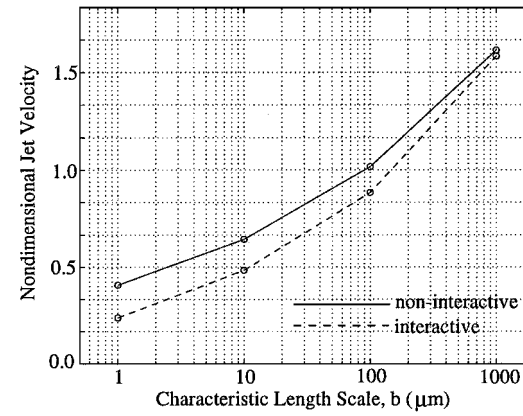

Fig. 3 Optimized nondimensional maximum jet exit velocity vs actuator scale b. Boundary-layer characteristics are as for Fig. 2. Actuator specifications: $d_c = 50b$, $h_c = 100b$, and $\ell = 2.5b$.

characteristics are the same as before. It is clear that as b is reduced there is an increasing difference between the values predicted for the maximum jet velocity with and without account taken of the presence of the boundary layer. The optimum values of d_e will also be different. It is necessary to treat these results with caution, however, as the optimized maximum jet speeds probably greatly exceed the limits of validity of the linearized simulations, especially at the larger scales. But there is no reason to doubt the validity of the overall conclusion; namely, that in order to obtain realistic results, fully coupled simulations become increasingly necessary as the dimensions of the actuator become smaller. The actuator size for controlling the near-wall turbulent structures at flight conditions corresponds to approximately $b = 1\ \mu$m.

It is also striking in Fig. 2 that whether we consider the actuator in isolation or interacting with the boundary layer there is an inflow phase after the initial jet outflow. At first sight this may seem rather surprising. It occurs as a result of Helmholtz resonance.[18] Essentially, this is a resonant oscillation of the cavity/orifice system. It is clear that, if inflow is undesirable, this phenomenon will have to be understood and avoided. Unfortunately, optimizing pressure-jump actuators involves a tradeoff between maximizing pressure rise and minimising viscous losses in the exit nozzle. This is very similar to the conditions for producing Helmholtz resonance, which is suppressed when viscous effects are too strong. Our parametric studies[18] reflect this tradeoff and show that when actuators are optimized for maximum jet velocity they are invariably susceptible to Helmholtz resonance. For synthetic jets the optimum design appears to be obtained when the Helmholtz frequency coincides with the natural frequency of the diaphragm. Helmholtz resonance in jet-type actuators and its consequences will be explored in more detail in a subsequent paper.

Up to this point it has been tacitly assumed that the maximum jet exit velocity should be as large as possible to obtain the best actuator performance. It is by no means obvious that this is the quantity that should be maximized. In an attempt to elucidate this point, we undertook a parametric study of the receptivity of two-dimensional Tollmien–Schlichting waves to two-dimensional pufflike jets. In this case the time-dependent velocity profiles were specified (in a similar way to Fig. 4) so that only outflow occurred. It was necessary to choose some measure of the instantaneous magnitude of the flow perturbation so generated. It would have been possible to choose the maximum magnitude of perturbation velocity or vorticity. But such a pointwise measure would not take into account the spatial extent of the perturbation and this could vary from case to case. It therefore seemed preferable to choose a global measure. Possible choices would be the total kinetic energy or enstrophy of the disturbance. But their evaluation would require volume integration (i.e., an area integration in the present two-dimensional case) over the whole disturbed domain. A suitable choice, that reflects the spatial extent of the disturbance but only requires an area integration (i.e., a line integration in the present two-dimensional case), is the integral of ω^2 over the wall. We have termed this quantity wall enstrophy.

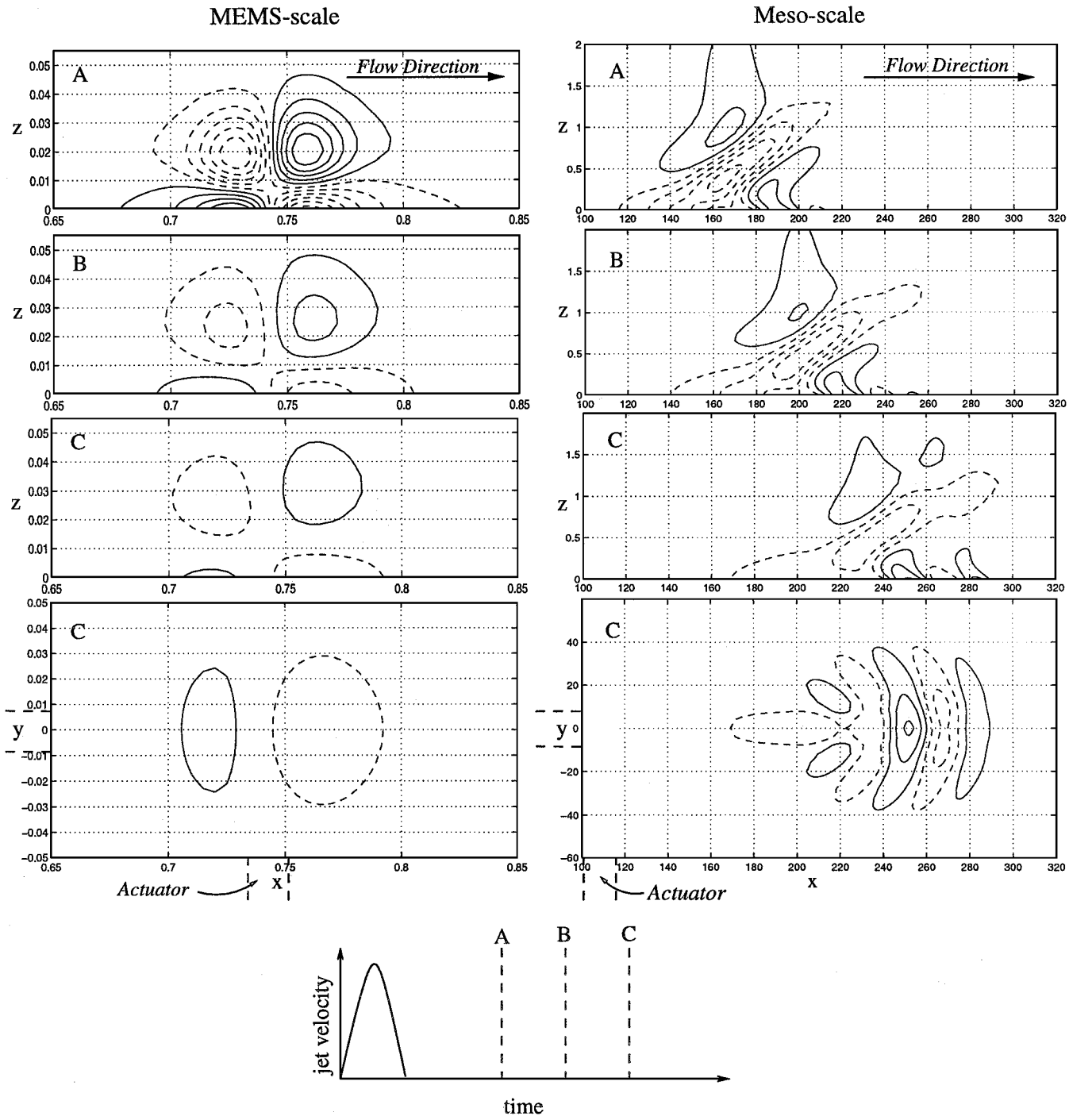

Fig. 4 Comparison between the evolution of boundary-layer perturbations generated by MEMS- and mesoscale actuators. The maximum jet velocity is 4 m/s, U_∞ = 30 m/s, δ^* = 1 mm, and R = 2000 in both cases. The actuator exit diameter $d_e = 0.016\delta^*$ and $16\delta^*$ for MEMS- and mesoscale, respectively, and the jet duration is $6.25d_e/U_\infty$ in both cases. The coordinates are given in millimeters. The plots show contours of spanwise perturbation vorticity at three different nondimensional times; - - - -, negative values; and the planform contours at time C are for $z = 0$. For the meso-scale simulations the nth contour is at $\pm(0.5 + n)$, and for the MEMS-scale the nth contour is at $\pm(2.5 + 5n) \times 10^{-3}$.

Figure 5 plots wall enstrophy as a function of time. In all cases shown this quantity reaches a minimum before starting to rise again at later times. The rising wall enstrophy indicates that the receptivity process is complete and exponentially growing Tollmien–Schlichting waves have been initiated. We regard the magnitude of this minimum as being a measure of the efficiency of receptivity; the larger it is, the greater the effective initial amplitude of the Tollmien–Schlichting waves. For any particular configuration we can always increase the receptivity by, for example, increasing the maximum jet velocity keeping the duration fixed. It is also true that receptivity would be greatest for exit nozzles similar in size to the Tollmien–Schlichting wavelength. But we wished to ascertain what choice of jet characteristic (for example, total mass, momentum, or kinetic energy outflow, or maximum velocity) would best reflect the capacity of the actuator to generate boundary-layer disturbances. Accordingly what we did was fix the exit jet width and vary the maximum velocity and duration of the jet in such a way as to keep certain overall jet characteristics (such as total mass, momentum, or energy flow) unchanged. The solid line shows the datum case. When we varied the maximum jet velocity and duration in such a way as to keep the total mass flow ejected fixed, no departure from the datum was observed. This implies that the receptivity is not affected by changes in total momentum or energy flux, providing the total mass flow does not change. Whereas when the total momentum or energy ejected was kept fixed, it is evident from Fig. 5 that there were considerable departures from the datum case;

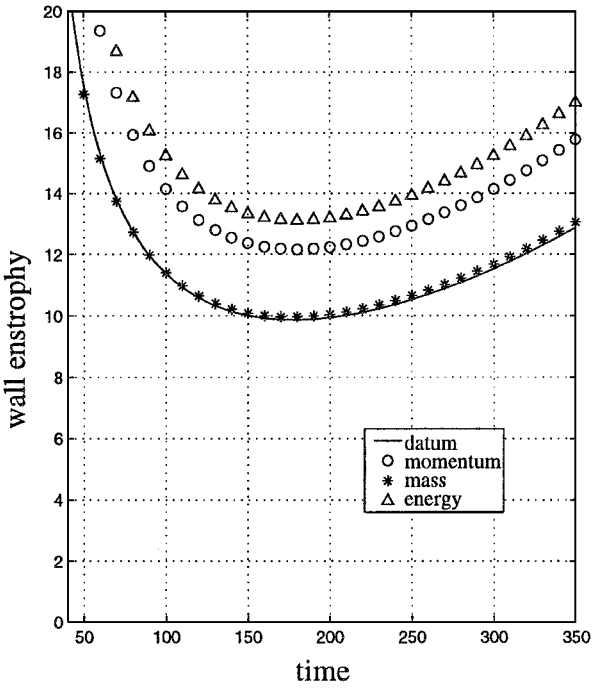

Fig. 5 Variation with time of the wall enstrophy of the perturbation produced by a transient two-dimensional jet-type actuator. The jet exit velocity was specified as a function of time and varied so as to keep various specified overall jet characteristics invariant. For all cases U_∞ = 30 m/s and R = 2000. For the datum case the maximum jet velocity is $0.1U_\infty$, the duration of the jet is $10\delta^*/U_\infty$, and the actuator exit width is $10\delta^*$.

in fact, the minimum wall enstrophy increased compared with the datum. This was because the total mass outflow was greater than the datum value, even though the total momentum or energy outflows remained unchanged. Similar departures from the datum case were observed for a number of other jet characteristics, such as maximum velocity, for example. We therefore conclude that total ejected mass flow is the best overall characteristic to maximize for the generation of two-dimensional Tollmien–Schlichting waves. It also turns out to be the best choice for the three-dimensional Klebanoff modes, which can be regarded as prototype sublayer streaks.[18]

Finally, we investigate the differences between the boundary-layer responses to mesoscale actuators and similar MEMS devices. Such differences have already been touched on in the discussion of Fig. 3. Figure 4 compares the forms of the perturbations in the two cases. The jet exit velocity profile is specified as parabolic in shape with $\tilde{w}_{\rm em}$ varying with time as shown in Fig. 4. In both cases $\tilde{w}_{\rm em}$ reaches the same maximum value of 4 m/s. For the MEMS and mesoscale actuators $d_e = 0.016\delta^*$ and $16\delta^*$, respectively; in both cases the duration of the jet is $6.25d_e/U_\infty$, $U_\infty = 30$ m/s, and $R = 2000$. Figure 4 shows the development of the boundary-layer disturbance in the two cases. It is plain that there are profound differences. In the case of the mesoscale actuator, the initial jetlike pertubation can be clearly discerned and moves downstream over the developing Tollmien–Schlichting wave packet. But with the MEMS device the initial jet-like perturbation remains in the vicinity of the orifice. No wave packet appears to develop. From the classic theoretical and experimental study of Gaster[19] and Gaster and Grant,[20] one would expect that a Tollmien–Schlichting wave packet would eventually develop downstream from a point impulsive source. Thus one may well eventually see such a wave packet evolving at large times for the MEMS actuator. Because of the great disparity in size between a MEMS actuator and the Tollmien–Schlichting wavelength, one would need a computational domain of the order of 10,000 d_e in length with corresponding spanwise dimensions to track the evolution of the wave packets in this case. This proved too demanding for our computational resources. But, by carrying out repeated rescaling of the computational domain, we were able to show[18] that a Tollmien–Schlichting wave packet was eventually generated at large times by a comparable two-dimensional MEMS actuator.

IV. Conclusions

We have developed a theoretical model for MEMS- and mesoscale actuators of the type whereby a force is applied to a diaphragm that then expels air from a cavity through an orifice into a laminar boundary layer. This model is used for a computational study of the interaction between such actuators and a laminar boundary layer. This study has led to the following main practical conclusions:

1) The perturbation in the boundary layer generated by the actuator can have a strong effect on the jet exit velocity from the orifice. This effect becomes increasingly strong as the actuator is reduced in size.

2) Actuators designed for peak performance are susceptible to Helmholtz resonance. Accordingly, even when the diaphragm is driven with a short-duration constant force, it is possible to have inflow into the cavity after the initial expulsion of air into the boundary layer.

3) For generating two-dimensional Tollmien–Schlichting waves, at least, the total mass expelled by the actuator appears to be the best overall characteristic to maximize.

4) When the evolutions of boundary-layer perturbations created by a mesoscale actuator (dimensions comparable to boundary-layer thickness) and MEMS-scale actuators (three orders of magnitude smaller) are compared over timescales based on actuator dimensions, great differences are revealed.

In our recent work[18] based on similar numerical-simulation techniques, we have investigated the effects of Helmholtz resonance on MEMS- and mesoscale actuators, including the generation of strong boundary-layer disturbances by "inactive" actuators excited by background noise. We have also developed a more complete computational model of a jet-type actuator that includes the dynamics of the piezoceramic driver. The input for this model is the voltage signal supplied to the driver and the output is the time-varying velocity profile at the orifice exit. Design optimization has been carried out based on this model and the results compared with empirically optimized actuators. Lastly, we have recently studied the control of the near-wall sublayer streaks in turbulent boundary layers using MEMS-scale jet-type actuators. These investigations will be described in subsequent papers.

Acknowledgments

The research reported here was undertaken as part of the AEROMEMS project (an investigation into the viability of MEMS technology for boundary-layer control on aircraft), which is a collaboration between British Aerospace; Dassault Aviation; Centre National de la Recherche Scientifique; and the Universities of Warwick, Manchester, Berlin, Madrid, Athens, Lausanne, and Tel-Aviv. The project is managed by British Aerospace and is partially funded by the CEC under the IMT initiative (Project Ref: BRPR CT97-0573).

References

[1] Gad-el-Hak, M., "The Fluid Mechanics of Microdevices—The Freeman Scholar lecture," *Journal of Fluids Engineering*, Vol. 121, No. 1, 1999, pp. 5–33.

[2] Löfdahl, L., and Gad-el-Hak, M., "MEMS Applications in Turbulence and Flow Control," *Progress in Aerospace Sciences*, Vol. 35, No. 2, 1999, pp. 101–203.

[3] Rathnasingham, R., and Breuer, K. S., "Coupled Fluid-Structural Characteristics of Actuators for Flow Control," *AIAA Journal*, Vol. 35, No. 5, 1997, pp. 832–837.

[4] Smith, B. L., and Glezer, A., "The Formation and Evolution of Synthetic Jets," *Physics of Fluids*, Vol. 10, No. 9, 1998, pp. 2281–2297.

[5] Rizzetta, D. P., Visbal, M. R., and Stanek, M. J., "Numerical Investigation of Synthetic-Jet Flowfields," *AIAA Journal*, Vol. 37, No. 8, 1999, pp. 919–927.

[6] Crook, A., Sadri, A. M., and Wood, N. J., "The Development and Implementation of Synthetic Jets for the Control of Separated Flow," AIAA Paper 99-3176, June 1999.

[7] Amitay, M., Smith, D. R., Kibens, V., Parekh, D. E., and Glezer, A., "Aerodynamic Flow Control over an Unconventional Airfoil Using Synthetic Jet Actuators," *AIAA Journal*, Vol. 39, No. 3, 2001, pp. 361–370.

[8] Seifert, A., Bachar, T., Koss, D., Shepshelovich, M., and Wygnanski, I., "Oscillatory Blowing: A Tool to Delay Boundary-Layer Separation," *AIAA Journal*, Vol. 31, No. 11, 1993, pp. 2052–2060.

[9]Nishri, B., and Wygnanski, I., "Effects of Periodic Excitation on Turbulent Flow Separation from a Flap," *AIAA Journal*, Vol. 36, No. 4, 1998, pp. 547–556.

[10]Seifert, A., and Pack, L. G., "Oscillatory Control of Separation at High Reynolds Number," *AIAA Journal*, Vol. 37, No. 9, 1999, pp. 1062–1071.

[11]Jacobson, S. A., and Reynolds, W. C., "Active Control of Streamwise Vortices and Streaks in Boundary Layers," *Journal of Fluid Mechanics*, Vol. 360, 1998, pp. 179–211.

[12]Lachowicz, J. T., Yao, C., and Wlezin, R. W., "Flow Field Characteristics of a Jet and Vortex Actuator," *Experiments in Fluids*, Vol. 27, No. 1, 1999, pp. 12–20.

[13]Hassan, A. A., and JanakiRam, R. D., "Effects of Zero-Mass 'Synthetic' Jets on the Aerodynamics of the NACA-0012 Airfoil," *Journal of the American Helicopter Society*, Vol. 43, No. 4, 1998, pp. 303–311.

[14]Carlson, H. A., and Lumley, J. L., "Flow over an Obstacle Emerging from the Wall of a Channel," *AIAA Journal*, Vol. 34, No. 5, 1996, pp. 924–931.

[15]Hoffmann, L. M., and Herbert, Th., "Disturbances Produced by the Motion of an Actuator," *Physics of Fluids*, Vol. 9, No. 12, 1997, pp. 3727–3732.

[16]Davies, C., and Carpenter, P. W., "Numerical Simulation of the Evolution of Tollmien–Schlichting Waves over Finite Compliant Walls," *Journal of Fluid Mechanics*, Vol. 335, 1997, pp. 361–392.

[17]Davies, C., and Carpenter, P. W., "A Novel Velocity-Vorticity Formulation of the Navier-Stokes Equations with Application to Boundary-Layer Disturbance Evolution," *Journal of Computational Physics*, Vol. 172, 2001, pp. 119–165.

[18]Lockerby, D. A., "A Numerical-Simulation Study of Boundary-Layer Control Using MEMS Actuation," Ph.D. Dissertation, School of Engineering, Univ. of Warwick, Coventry, England, U.K., March 2001.

[19]Gaster, M., "A Theoretical Model of a Wave Packet in the Boundary Layer on a Flat Plate," *Proceedings of the Royal Society London*, Vol. A347, April 1975, pp. 271–289.

[20]Gaster, M., and Grant, I., "An Experimental Investigation of the Formation and Development of a Wave Packet in a Laminar Boundary Layer," *Proceedings of the Royal Society London*, Vol. A347, April 1975, pp. 253–269.

P. J. Morris
Associate Editor